

Photocatalytic hydrogen production by water splitting using novel catalysts under UV-vis light irradiation

Francisco Márquez^{*1}, Antonio Masa¹, María Cotto¹, Abraham García¹, José Ducongé¹, Teresa Campo², Eduardo Elizalde² and Carmen Morant²

¹Nanomaterials Research Group-NRG, School of Science and Technology, University of Turabo, 00778 PR, USA

²Departamento de Física Aplicada, M-XII, Universidad Autónoma de Madrid, Cantoblanco, 28049 Madrid, Spain

(Received November 19, 2013, Revised March 12, 2014, Accepted March 12, 2014)

Abstract. Photocatalytic hydrogen generation by water splitting ($\text{H}_2\text{O}_{(l)} \rightarrow \text{H}_{2(g)} + 1/2\text{O}_{2(g)}$) has been studied on photocatalysts based on Zn, Cd, Fe and Cu, synthesized by coprecipitation. Iron and copper nanoparticles were incorporated as cocatalysts to enhance the photocatalytic activity of the ZnCd solid solution. The effect of the different synthesis parameters (temperature, elemental atomic ratios, amount of Cu and Fe incorporated in the catalyst and calcination temperature) on the photocatalytic production of hydrogen has been studied in order to determine the best experimental synthesis conditions. The catalysts have been characterized by X-ray diffraction (XRD), scanning electron microscopy (SEM), X-ray photoelectron spectroscopy (XPS), and BET. The experiments of photocatalytic water splitting were performed in aqueous solution of the photocatalysts previously dispersed in a soft ultrasound bath. The photocatalysts were irradiated under different lights ranging from 220 to 700 nm. The photocatalytic activity was found to be clearly dependent on the specific area of the photocatalyst.

Keywords: Hydrogen production; water splitting; photocatalyst; nanowires; solid solution

1. Introduction

Photocatalytic water splitting with generation of hydrogen is a green process that concerns activity of a semiconductor material under sunlight irradiation and ambient pressure and temperature. This process has been regarded as a promising solution to resolve the global energy and environmental problems (Kalyanasundaram *et al.* 1978). Nevertheless, the most of the photocatalysts can only be used in a short wavelength range, in ultraviolet region or near to that. Thermodynamically, the water splitting reaction is an uphill process characterized by a highly positive Gibbs free energy ($G^\circ = +238 \text{ kJmol}^{-1}$) (Bamberger *et al.* 1976). In this process, the photocatalyst is the component capable of absorbing the energy to drive the splitting reaction



*Corresponding author, Associate Professor, E-mail: fmarquez@suagm.edu

Since the landmark work of Honda and Fujishima in 1972 on the photoelectrochemical splitting of water using TiO_2 as catalyst (Fujishima *et al.* 1972), a vast body of literature describing this process has been developed (Navarro *et al.* 2009, Kudo *et al.* 2009 and Maeda *et al.* 2007 and Osterloh 2008). Over 140 different new catalysts including multicomponent oxides, sulfides or nitrides, have been synthesized for driving this reaction, and in all cases, has been demonstrated that the conversion efficiency is a function of a large number of factors, including how much the sunlight is absorbed, the energy of the absorbed photons, the efficiency of transforming absorbed photons in separated electrons and holes, how the carriers are moved through the material to the catalyst surface, and how these separated electrons and holes are transferred to produce the desired products (in the present case, hydrogen and oxygen) (Grimes *et al.* 2008, Bard 1980, Bard *et al.* 1995, Lewis 1990 and Nozik *et al.* 1996). In recent years there has been an increasing interest for using mixed metal oxides solid solutions as heterogeneous catalysts, since the combination of several metals in a homogeneous matrix can give rise to improved structural and electronic properties with potential applications in hydrogen production. In this research we have determined that CdZnFeS and CdZnFeCuS mixed oxides catalysts can be efficiently used as photocatalysts to generate hydrogen from photocatalytic water splitting. With the aim to improve the hydrogen production, these mixed oxides catalysts were supported on TiO_2 nanowires (TiO_2NWs) previously synthesized. Pristine and supported mixed oxides based catalysts have been characterized using X-ray diffraction (XRD), X-ray photoelectron spectroscopy (XPS), UV-visible spectroscopy, scanning electron microscopy (SEM), and BET surface analysis. It is believed that the methods of preparation, and specifically the thermal treatment conditions, affect the crystallinity and specific area of the photocatalysts and subsequently the activity in the water splitting reaction.

2. Materials & methods

2.1 Chemicals

All chemicals were of analytical grade and used as received without any further purification, unless otherwise described. CuO (99.9% purity) was provided by Merck Chemicals (Merck, KGaA, Darmstadt, Germany). $\text{Cd}(\text{CH}_3\text{COO})_2$ (99.9% purity) and $\text{Zn}(\text{CH}_3\text{COO})_2$ were provided by Sigma-Aldrich and used as received. FeS (99.9% purity) was provided by Sigma-Aldrich Co. (Germany). $\text{Na}_2\text{S}\cdot 9\text{H}_2\text{O}$ (> 98% purity) and Na_2SO_3 (> 98% purity) were provided by Sigma-Aldrich (USA). Pure ethyl alcohol was provided by Aldrich Chemical (USA). Milli-Q water (> 18.2 $\text{M}\Omega\cdot\text{cm}$ resistivity at 25 °C) was used for all experiments.

2.2 Synthesis of catalysts

2.2.1 ZnCdFeS mixed oxide solid solution

The ZnCdFeS mixed oxide catalyst was synthesized by co-precipitation of equimolar CdS and ZnS aqueous solution using FeS as precipitating agent (Navarro *et al.* 2009). The precursors $\text{Cd}(\text{CH}_3\text{COO})_2$ and $\text{Zn}(\text{CH}_3\text{COO})_2$ were dissolved in deionized water to obtain 0.3 M solutions (Navarro *et al.* 2009). After that, both solutions were mixed during 20 min in a soft ultrasound bath at temperatures ranging from rt to 60 °C. Next, FeS (5% in water) was added to the reaction

mixture and maintained in the ultrasound bath for 40 min. The precipitate obtained is separated from the solution by centrifugation (4000 rpm 20 min) and washed repeatedly with deionized water (five cycles) and with ethanol (two cycles). The synthesized compound was dried overnight at 80 °C and thermally treated at different temperatures in flowing nitrogen.

2.2.2 ZnCdFeCuS mixed oxide solid solution

The synthesis process includes the addition of CuNO_3 as precursor of Cu into the solid solution (Masa *et al.* 2011). Similarly, precursors were dissolved in deionized water to obtain 0.3 M solutions. After that, solutions were mixed during 20 min in an ultrasound bath at temperatures ranging from rt to 60 °C. Next, $\text{Na}_2\text{S}\cdot 9\text{H}_2\text{O}$ (5% in water) was added to the reaction mixture and maintained in a soft ultrasound bath for 50 min. The precipitate obtained is separated from the solution by centrifugation (5000 rpm 30 min) and washed repeatedly with deionized water (five cycles) and with ethanol (two cycles). The synthesized compound was dried overnight at 80 °C and thermally treated at different temperatures in flowing nitrogen.

2.2.3 ZnCdFeS@TiO₂ NWs and ZnCdFeCuS@TiO₂ NWs

These catalysts were synthesized by using the method of impregnation and drying. The precursors (ZnCdFeS and ZnCdFeCuS nanoparticles) were ground finely and dispersed in ethanol (20 mg of nanoparticles in 30 ml of ethanol) in an ultrasound bath (750 W, 20 min). Next, these solutions were added to 60 mg of TiO₂NWs previously synthesized. The mixtures were homogeneously mixed for 20 min using a shaker and dried at 50 °C for 2 days. Finally, the resulting catalysts (ZnCdFeS@TiO₂NWs and ZnCdFeCuS@TiO₂NWs) were calcined at 400 °C in flowing nitrogen for 2 hours.

The synthesis of TiO₂NWs is based on a sol-gel reaction (Cotto *et al.* 2011). Thus, for a typical synthesis, 1 mL of Ti tetrachloride was dissolved in 20 mL of HCl:H₂O (1:1); the solution was magnetically stirred at room temperature for 1 hr. Then, 0.1 mL of Ti (IV) isopropoxide is added drop-wise under constant stirring for 15 min. The resulting reaction mixture was stirred for 1 h at room temperature. The solution was placed into a Teflon-lined stainless steel autoclave of 30 mL capacity and maintained at 170 °C by 12 hours. After cooling to room temperature, the white sediment is collected and washed in water by five centrifugation (5000 rpm, 15 min)-redispersion cycles. Next, the powder was resuspended in ethanol and washed by three centrifugation (6000 rpm, 6 min)-redispersion cycles. Finally, the TiO₂NWs were suspended in ethanol and dried overnight at 60 °C.

2.3 Characterization

X-ray powder diffraction patterns (XRD) were collected using an X Pert PRO X-ray diffractometer (PANalytical, The Netherlands) in Bragg-Brentano goniometer configuration. The X-ray radiation source was a ceramic X-ray diffraction Cu anode tube type Empryan of 2.2 kW. XRD diffractograms were recorded in angular range of 5-110 degrees.

Scanning electron microscopy (SEM) images were obtained using a Field Emission-SEM (Philips, FEG-XL30S, 20 kV, Philips Electronic Instruments Co., Chicago, IL, USA) and a SEM (JSM-6010LA, 20 kV, JEOL USA Inc).

XPS measurements were performed on an ESCALAB 220i-XL spectrometer, by using the non-monochromated Mg K α (1253.6 eV) radiation of a twin-anode, operating at 20 mA and 12 kV in

the constant analyzer energy mode, with a PE of 50 eV. To avoid the X-ray induced changes in the oxidation states (i.e. reduction of Cu^{+2} to Cu^{+1}) samples were maintained at 173 K during the acquisition and the X-ray power was limited to 200 W. The spectral acquisition time was also reduced to the maximum to prevent the damage of the sample and the possible reduction of Cu^{+2} . In order to remove charging shifts and deal with Fermi edge coupling problems, binding energies were corrected using the peak of the C-(C,H) component coming from contamination carbon (set to 284.6 eV). The samples were pressed onto a molybdenum support and then were put into the preparation chamber to pump for approximately ZA24 h at 60 °C under a pressure of about 10^{-7} Pa to minimize surface contamination. Small amounts of activated carbon fine powder were added to the samples to improve their conductivity. The vacuum during spectra acquisition was better than 5×10^{-9} mbar.

The atomic concentrations in outer surface layers of the samples were estimated from the corresponding XPS peak area ratios using the equation

$$\left[\frac{X}{Y} \right]_S = \frac{A_{(X)} \sigma_{(Y)} \lambda_{(Y)}}{A_{(Y)} \sigma_{(X)} \lambda_{(X)}} \sqrt{\frac{E_{K(X)}}{E_{K(Y)}}}$$

where A is the integral of each peak after S-shaped background subtraction, σ is the effective ionization cross section, λ is the escape depth, and E_K is the photoelectron kinetic energy. Cross section values were taken from Scofield (Scofield 1976) and the escape depth were calculated from the formulas given by Vulli and Starke (Vulli *et al.* 1978).

Nitrogen physisorption was performed at 77 K using a Micromeritics ASAP 2020. The experimental data were used to determine the BET surface area. Prior to the physisorption measurements, the samples were dried overnight at 473 K under nitrogen atmosphere.

Quantification of the evolved gases was performed by using a gas chromatograph equipped with a thermal conductivity detector (GC-TCD, Agilent 6890). A 5 Å molecular sieve column (2 m length \times 2 mm i.d.) with N_2 as the carrier gas was used to separate the gases produced in the catalytic reactions.

2.4 Catalytic tests

Before use, the catalysts were either activated under a nitrogen flow of 300 mL min^{-1} at different temperatures (400, 700 and 900 °C) for 2 hours. In all cases, the photocatalytic activity was measured by dispersing 50 mg of the catalyst in deionized water in an ultrasound bath at room temperature and atmospheric pressure containing 0.5 M Na_2S and 0.03 M Na_2SO_3 as sacrificial reagents. In the different catalysts tested, the catalytic peak for the overall water splitting reaction occurs in a short pH range, typically 4-5.2 and for this reason, solutions were pH-adjusted. The reaction mixture was purged with $\text{N}_{2(g)}$ for 20 min and after that evacuated several times to completely remove the air prior the irradiation process. The water splitting reaction was conducted in a quartz reactor equipped with a water-cooling jacket. The reaction mixtures were irradiated at different light wavelengths (from 220 to 700 nm) using a solar simulator and appropriate cutoff filters in a static air atmosphere. To facilitate the catalyst dispersion in the reactant solutions, a magnetic stirrer was used. The evolved gases were analyzed by gas chromatography with a thermal conductivity detector using N_2 as carrying gas.

3. Results and discussion

3.1 Characterization of the as-prepared catalysts

The synthesized catalysts were characterized by BET, SEM, XRD and XPS. Tables 1 and 2 show the atomic compositions and BET surface areas of the catalysts synthesized at different temperatures. As can be seen there, the atomic percentages of Zn, Cd, Fe, S and Cu depend on the synthesis temperature. Synthesis temperature above 60 °C produced catalysts whose particles showed inhomogeneous composition (as evidenced by EDX and XPS).

Catalysts synthesized at 60 °C show higher BET areas than those obtained at lower temperatures and for this reason these catalysts have been selected as the most appropriate for this research. In this way, SAM-4 and SAM-8 were dispersed by impregnation on TiO₂NWs giving rise to two new catalysts (ZnCdFeS@TiO₂NWs and ZnCdFeCuS@TiO₂NWs) that were identified as SAM-4A and SAM-8A respectively. The BET areas of these catalysts are clearly higher than those observed for the starting materials, with values ranging from 235 to 244 m²g⁻¹ (see Table 3).

Fig. 1 shows the SEM images corresponding to the ZnCdFeS (Fig. 1(a)) and ZnCdFeCuS (Fig. 1(b)) mixed oxide catalysts previously synthesized.

In both catalysts the particle size ranged from ca. 10 to 15 nm. Figs. 1(c) and (d) shows the micrographs of the same catalysts after impregnation on TiO₂ NWs. As can be seen there, the presence of small nanoparticles of the mixed oxides on the surface of the nanowires is clearly observed, revealing a very high dispersion on the surface.

Table 1 Atomic composition and surface area BET of ZnCdFeS catalysts

Sample	Temperature(°C)	Zn(%)	Cd(%)	Fe(%)	S(%)	S _{BET} (m ² g ⁻¹)
SAM-1	25	31	21	8	40	164
SAM-2	35	29	21	6	44	112
SAM-3	50	25	22	5	48	101
SAM-4	60	20	18	9	53	178

Table 2 Atomic composition and surface area BET of ZnCdFeCuS catalysts

Sample	Temperature(°C)	Zn(%)	Cd(%)	Fe(%)	Cu(%)	S(%)	S _{BET} (m ² g ⁻¹)
SAM-5	25	12	13	12	28	35	146
SAM-6	35	15	10	12	27	36	153
SAM-7	50	17	9	12	25	37	158
SAM-8	60	19	11	15	24	31	181

Table 3 Atomic composition and surface area (BET) of SAM-4A (ZnCdFeS@TiO₂NWs) and SAM-8A (ZnCdFeCuS@TiO₂NWs) catalysts

Sample	Zn(%)	Cd(%)	Fe(%)	Cu(%)	S(%)	Ti(%)	S _{BET} (m ² g ⁻¹)
SAM-5	12	10	5	---	22	51	235
SAM-6	8	5	6	10	15	56	244

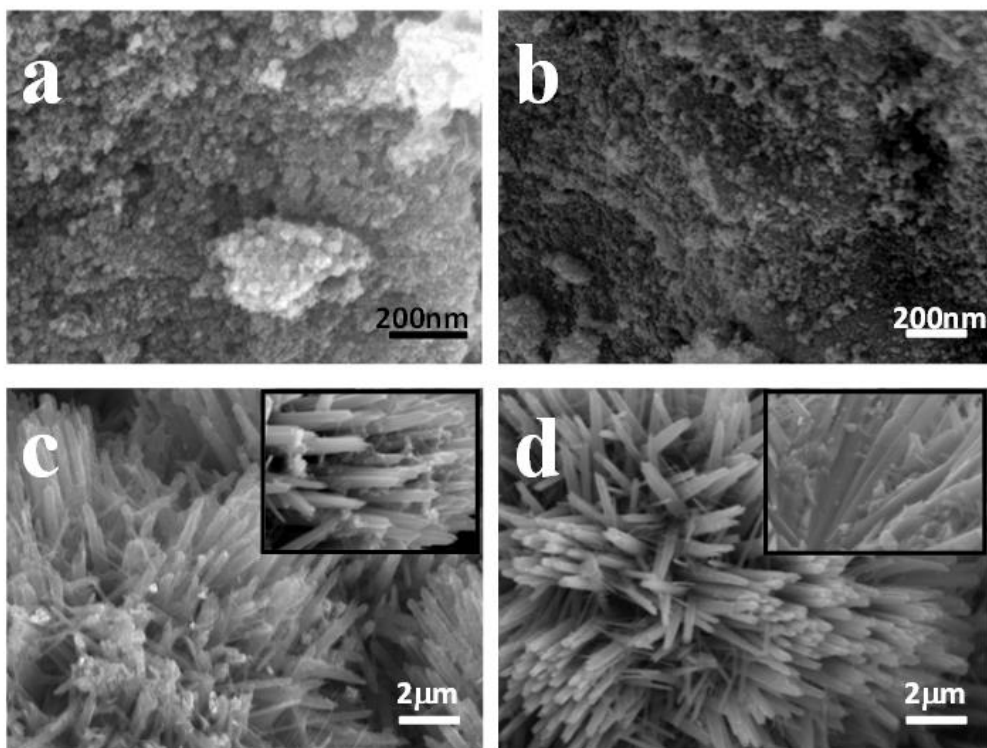


Fig. 1 SEM images of (a) ZnCdFeS, (b) ZnCdFeCuS, (c) ZnCdFeS@TiO₂NWs and (d) ZnCdFeCuS@TiO₂NWs. Insets of c and d show magnifications (X2) of the catalysts surfaces

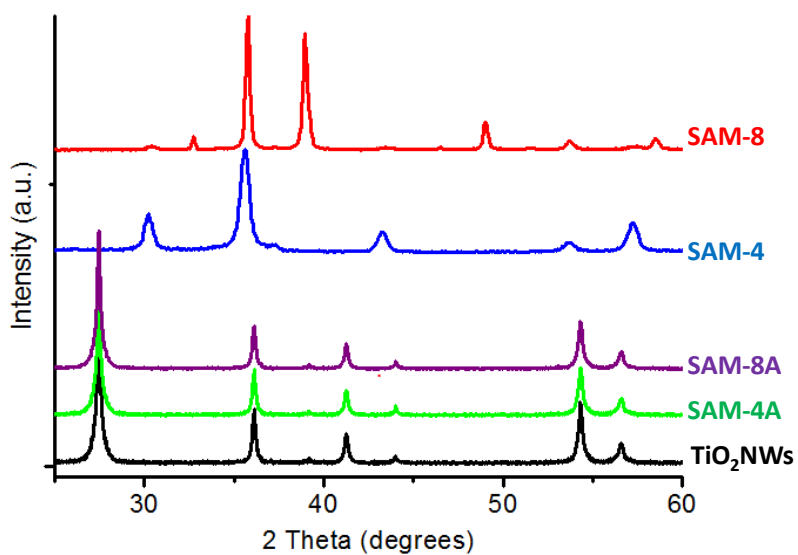


Fig. 2 XRD patterns of the catalysts studied. For comparison purposes the XRD pattern of TiO₂NWs is also given

The crystalline structure of the synthesized catalysts was studied by XRD. Fig. 2 shows the XRD patterns of samples SAM-4 and SAM-8. Both diffractograms are characterized by having reflections at intermediate positions to the corresponding ZnS and CdS precursors, indicating that these compounds have been synthesized as mixed oxide solid solutions (Navarro *et al.* 2009). On impregnation of SAM-4 and SAM-8 over TiO₂NWs (samples SAM-4A and SAM-8A) no characteristics peaks of the original ZnCdFeS or ZnCdFeCuS nanoparticles were observed and only the characteristics reflections of the rutile phase corresponding to the supporting material (TiO₂NWs) were identified (see Fig. 2). The absence of signals from SAM-4 and SAM-8 in SAM-4A and SAM-4B has been justified as due to the high dispersion of the precursors on TiO₂ NWs.

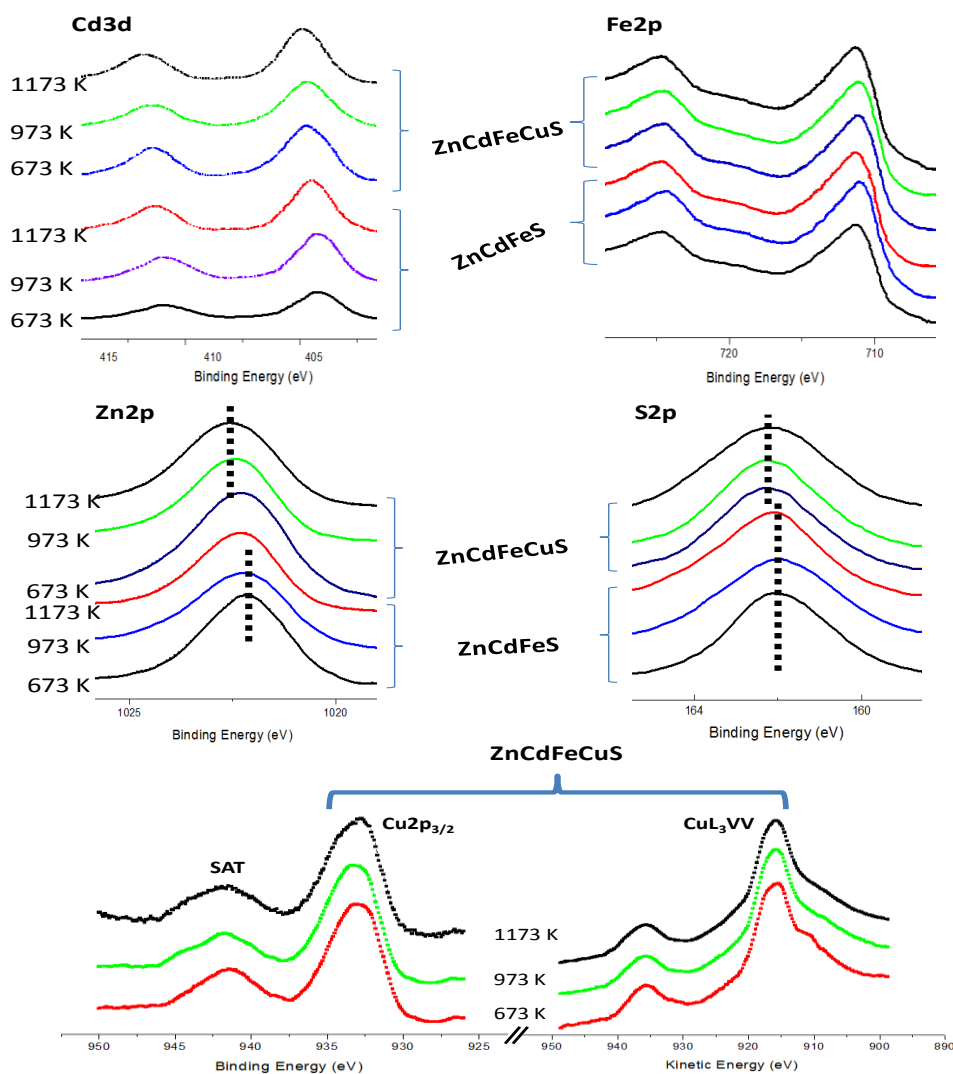


Fig. 3 XPS of catalysts SAM-4 (ZnCdFeS) and SAM-8 (ZnCdFeCuS), after annealing activation treatments in nitrogen at 400 °C, 700 °C and 900 °C

SAM-4 and SAM-8 were studied by XPS with the aim to characterize the chemical environment of the elements constituting the catalysts. The main regions corresponding to Cd3d, Fe2p, Zn2p, S2p, Cu2p and CuL₃VV after different temperature treatments in flowing nitrogen are shown in Fig. 3. As can be seen there, in all cases peaks corresponding to SAM-8 are slightly shifted to higher binding energies with respect to those measured for SAM-4. This effect could be justified as induced by the incorporation of copper to the mixed oxide solid solution. Moreover, the effect of temperature results in a shift to higher binding energies. This result may indicate that small changes in the coordination of the elements are possibly occurring during the thermal treatment.

All the XPS regions seem to indicate the presence of the different elements in the oxidation state of 2+. In the case of Cu2p, the effect of shifting of the BE under thermal treatment is not so clear and, apparently the peak measured after different treatment temperatures does not experience relevant changes. To identify the oxidation state of copper in the sample SAM-8 the CuL₃VV was also recorded. Surprisingly Cu2p transition (Fig. 3) of SAM-8 previously treated under nitrogen flow at different temperatures is characterized by having a main peak at 936 eV (BE) and a

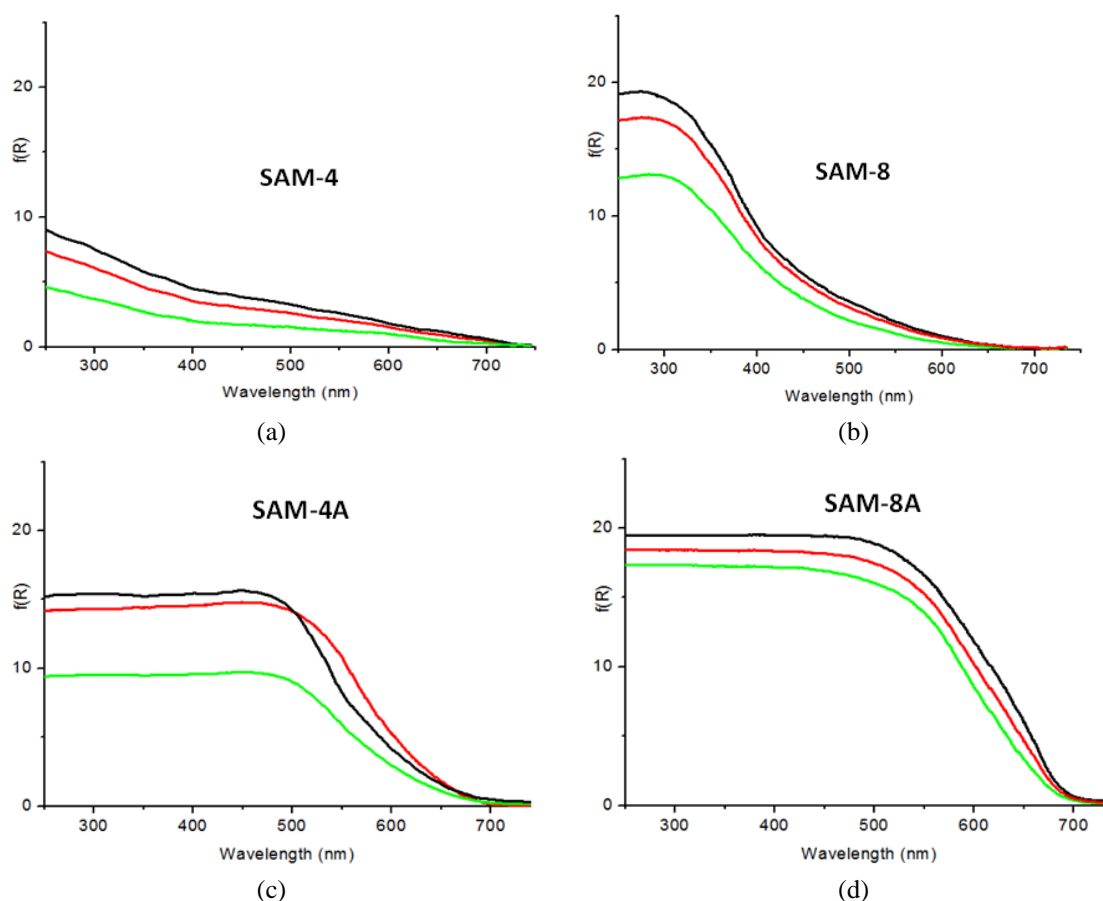


Fig. 4 UV-vis diffuse reflectance spectroscopy of (a) SAM-4, (b) SAM-4A, (c) SAM-8, and (d) SAM-8A, after annealing activation treatments in nitrogen at 400 °C (—), 700 °C (—), and 900 °C (—)

shake-up satellite at ca. 10 eV higher than the Cu(2p_{3/2}) transition. Only Cu⁺² species shows this shake-up and this result reflects that copper in this catalyst is present as Cu⁺², although the thermal treatment in a flow of nitrogen should produce at least the partial reduction of copper. The peak positions of the CuL₃VV Auger transition at ca. 916.5 eV (KE), after activation in a nitrogen flow at different temperatures, agrees with the presence of copper as Cu⁺².

A comparison of the UV-vis diffuse reflectance spectra of SAM-4, SAM-8, SAM-4A and SAM-8A is shown in Fig. 4. As can be seen there, the thermal treatment produces some changes that could be correlated with those observed in XPS. Thus, in all cases the higher reflectance is observed after activation at 700 °C in nitrogen. The incorporation of copper into the structure of SAM-4 (Fig. 4(a)) to obtain the catalyst SAM-8 (Fig. 4(c)) gives rise to an increased reflectance in the UV spectral range. The impregnation of these catalysts on the supporting material (TiO₂NWs) increases importantly the reflectance of visible light, producing a spectral shift to higher wavelengths (see Figs. 4(b) and (c)). This unexpected effect not yet clarified, may be justified because of the interactions of the catalyst nanoparticles with the support surface. Predictably, this spectral shift effect could have important implications for the efficiency and the performance of these catalysts in the water splitting reactions.

3.2 Catalytic activity

Photocatalytic hydrogen production studies were conducted on SAM-4, SAM-8, SAM-4A and SAM-8A catalysts. In all cases, control experiments showed no appreciable hydrogen production in absence of either the catalyst or irradiation source.

Fig. 5 shows the H₂ production on SAM-4, measured at room temperature, after different activation treatments in nitrogen at 400, 700 and 900 °C. As can be seen, the thermal treatment greatly affects the production of hydrogen. The catalyst requires an adequate temperature for the solid oxide mixed solution occurs. At 400 °C possibly the temperature is too low to promote the formation of the solid solution.

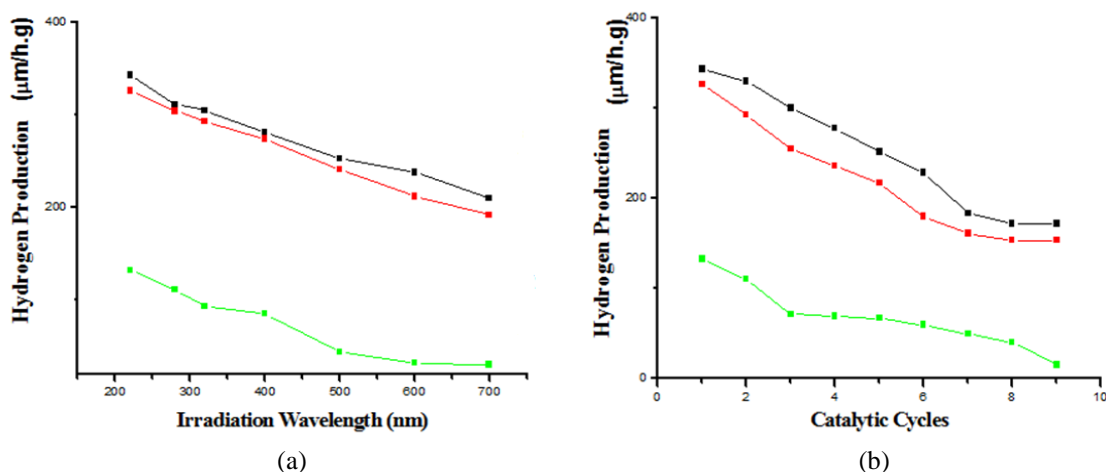


Fig. 5 (a) Hydrogen production over Sam-4 at different irradiation wavelengths, after annealing activation treatments in nitrogen at 400 °C (—■—), 700 °C (—■—) and 900 °C (—■—). (b) Recyclability of SAM-4 after nine consecutive reaction cycles

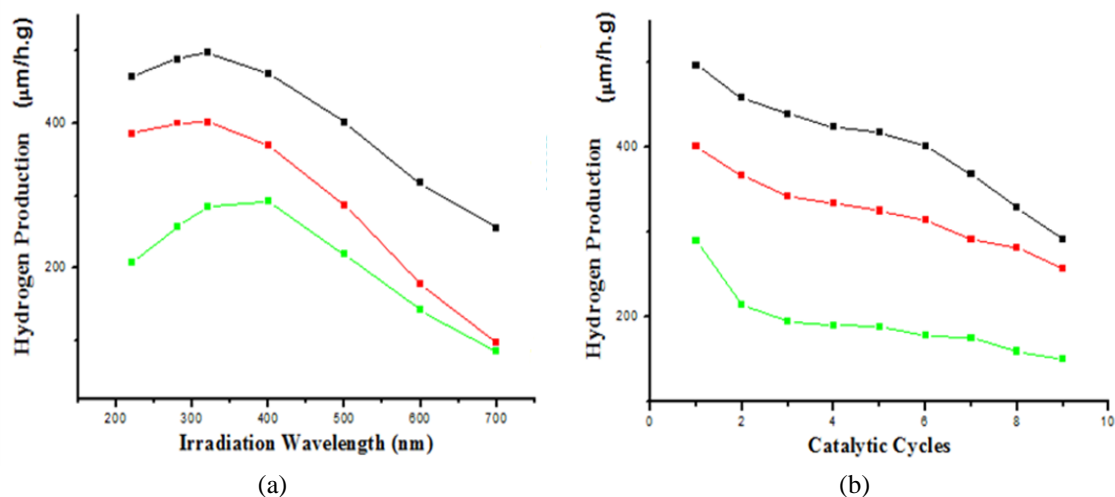


Fig. 6 (a) Hydrogen production over SAM-8 at different irradiation wavelengths, after annealing activation treatments in nitrogen at 400 °C (■), 700 °C (■) and 900 °C (■). (b) Recyclability of SAM-8 after nine consecutive reaction cycles

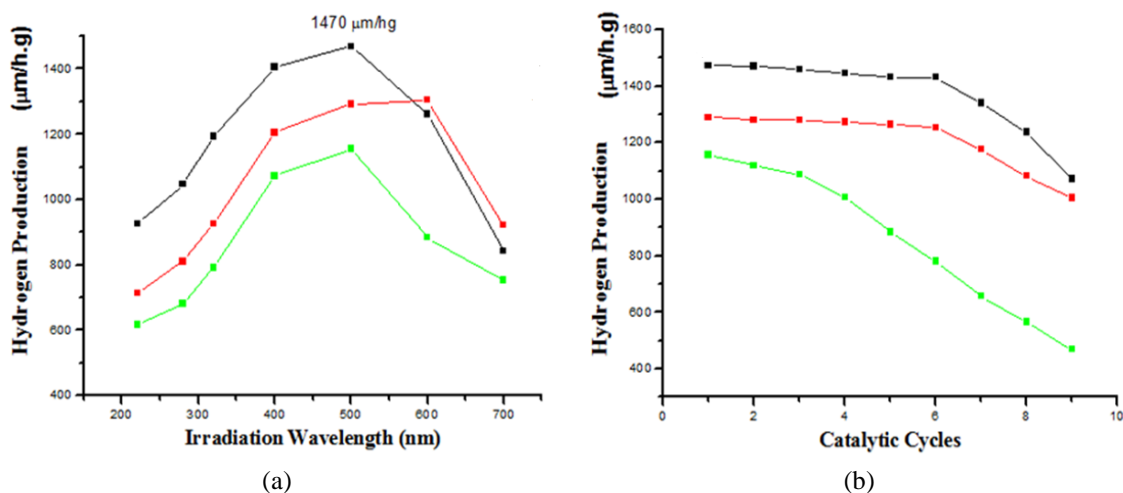


Fig. 7 (a) Hydrogen production over SAM-4A (ZnCdFeS@TiO₂NWs) at different irradiation wavelengths, after annealing activation treatments in nitrogen at 400 °C (■), 700 °C (■), and 900 °C (■). (b) Recyclability of SAM-4A after nine consecutive reaction cycles

At higher annealing temperatures (i.e. 700 or 900 °C) the crystallinity of the catalyst is improved and the solid solution is promoted, giving rise to the highest H₂ productions. In this catalyst the maximum H₂ production was measured under irradiation at 220 nm, with values near to 350 µmh⁻¹g⁻¹.

When the reaction is carried out with the catalyst SAM-8 (Fig. 6) the H₂ production after annealing in nitrogen at 700 °C increases up to 497 µmh⁻¹g⁻¹.

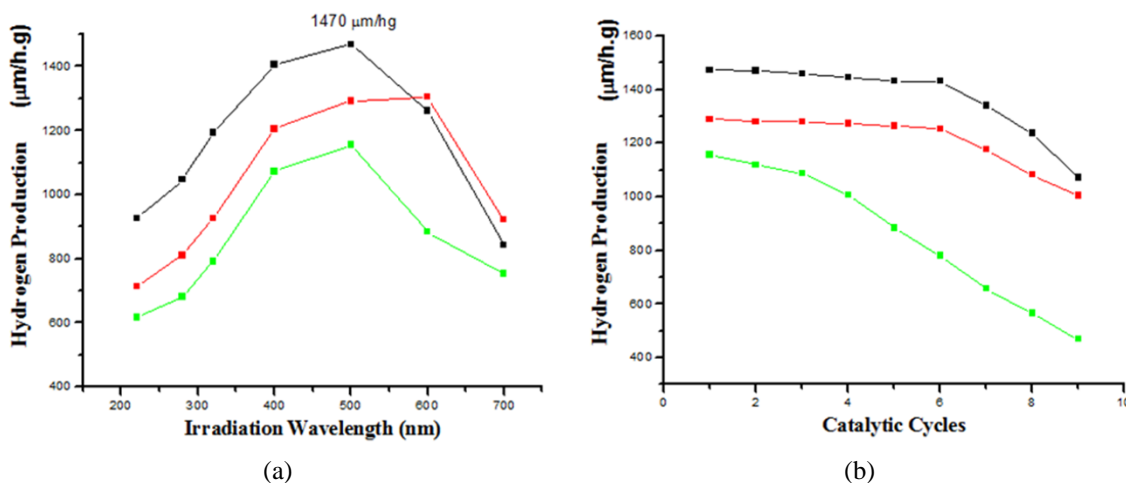


Fig. 8 (a) Hydrogen production over SAM-8A (ZnCdFeCuS@TiO₂NWs) at different irradiation wavelengths, after annealing activation treatments in nitrogen at 400 °C (■), 700 °C (■), and 900 °C (■). (b) Recyclability of SAM-8A after nine consecutive reaction cycles

In this case, the maximum production has been measured under irradiation at 320 nm. This red-shifting effect is presumably attributed to the incorporation of copper into the solid solution of the catalyst; this effect being more relevant after annealing at 400 °C with a maximum hydrogen production measured under irradiation at 400 nm.

Figs. 7 and 8 show the hydrogen evolution in presence of SAM-4A and SAM-8A, respectively. In both cases, the maximum H₂ production experiences an unexpected red-shift to the visible range of irradiation, with a maximum production at 500 nm (after annealing at 700 °C). This result could be correlated with the UV-vis diffuse reflectance measurements. Indeed, as seen in Figs. 4(b) and (d), the UV-vis absorption threshold of these catalysts drastically shifts to the red with respect to SAM-4 and SAM-8. In both catalysts the efficiency is considerably higher than in SAM-4 and SAM-8, this result being possibly due to the increased dispersion of the catalysts under impregnation on the TiO₂NWs support.

The recyclability of the catalysts was verified by submitting the same recovered catalysts to nine subsequent cycles of this reaction. In all cases, the hydrogen production was measured under irradiation at the most efficient wavelength. As can be seen in Figs. 5 and 6, an appreciable loss in activity was observed since the second reaction cycle. This activity loss clearly depends on the temperature of the annealing treatment. Catalytic activity in SAM-4 and SAM-8 undergoes a significant decrease, especially after annealing at 400 °C. In the case of catalysts SAM-4A and SAM-8A (Figs. 7 and 8, respectively), and as observed in SAM-4 and SAM-8, the activity loss depends on the annealing treatment but in these catalysts the recyclability is very good when samples are previously treated in nitrogen at 700 °C. At 400 °C apparently the usefulness of these catalysts, after several cycles of use, is somewhat limited. However, in both catalysts treated at 700 °C, the activity is practically not altered in SAM-4A and starts to decrease appreciably in SAM-8A from the seventh cycle of reuse. These effects are currently being studied and, at least in part, may be due to the leaching of some metal ions from the solid solution after several cycles of use.

4. Conclusions

We have synthesized a set of novel photocatalyst materials that have been tested for hydrogen generation from water by using irradiation sources ranging from 220 nm to 700 nm. In all catalysts studied the efficiency of hydrogen production was good. However, the highest generation rates were obtained with catalysts prepared by impregnation on TiO₂NWs. In these cases, the main reason for the increased activity could be the greatest degree of dispersion and the high surface area of the catalysts obtained by impregnation. The annealing temperature for the catalyst activation is essential for its activity. Relatively low processing temperatures (400 °C) are not sufficient for obtaining catalysts having good performance, being required higher treatment temperatures (700 °C) to achieve high levels of hydrogen production.

Acknowledgements

The authors gratefully recognize the financial support provided by Department of Energy through the Massie Chair project at University of Turabo. Financial support from MICINN (Spain) through the grant MAT2010-19804 is also acknowledged. AG thanks to School of Science and Technology and Puerto Rico Energy Center at University of Turabo for a teaching assistant fellowship. The “Servicio Interdepartamental de Investigación (SIIdI)” from Universidad Autónoma de Madrid, “Centro Nacional de Microscopia” from Universidad Complutense de Madrid, and Puerto Rico Energy Center are acknowledged for the use of the SEM and XRD facilities.

References

- Bamberger, C. and Richardson, D. (1976), “Hydrogen production from water by thermochemical cycles”, *Cryogenics*, **16**(4), 197-208.
- Bard, A.J. (1980), “Photoelectrochemistry”, *Science*, **207**(4417), 139-144.
- Bard, A.J. and Fox, M.A. (1995), “Artificial photosynthesis: Solar splitting of water to hydrogen and oxygen”, *Accounts. Chem. Res.*, **28**(3), 141-145.
- Cotto, M., Campo, T., Elizalde, E., Morant, C. and Márquez, F. (2011), “Hydrothermal synthesis and photocatalytic activity of titanium oxide nanowires”, *43rd IUPAC-world chemistry congress, Puerto Rico*.
- Fujishima, A. and Honda, K. (1972), “Electrochemical photolysis of water at a semiconductor electrode”, *Nature*, **238**(5358), 37-38.
- Grimes, C.A., Varghese, O.K. and Ranjan, S. (2008), *Light, water, hydrogen: The solar generation of hydrogen by water photoelectrolysis*, Springer, New York, NY.
- Kalyanasundaram, K., Kiwi, J.M. and Gratzel, M. (1978), “Hydrogen evolution from water by visible light. A homogeneous three component test system for redox catalysis” *Helv. Chim. Acta.*, **61**(7), 2720-2730.
- Kudo, A. and Miseki, Y. (2009), “Heterogeneous photocatalysts materials for water splitting”, *Chem. Soc. Rev.*, **38**, 253-278.
- Lewis, N.S. (1990), “Mechanistic studies of light-induced charge separation at semiconductor/liquid interfaces”, *Accounts. Chem. Res.*, **23**(6), 176-183.
- Maeda, K. and Domen, K. (2007), “New non-oxide photocatalysts designed for overall water splitting under visible light”, *J. Phys. Chem. C.*, **111**(22), 7851-7861.
- Masa, A., García, A., Cotto, M., Duong, J., Campo, T., Elizalde, E., Morant, C. and Márquez, F. (2011) “ZnCd-based photocatalysts for hydrogen production from water under visible-UV light”, *43rd*

IUPAC-world chemistry congress, Puerto Rico.

- Navarro, R.M., Álvarez, M.C., del Valle, F., Villoria, J.A. and Fierro, J.L.G. (2009), "Water splitting on semiconductor catalysts under visible-light irradiation", *Chem. Sus. Chem.*, **2**(6), 471-485.
- Nozik, A.J. and Memming, R. (1996), "Physical chemistry of semiconductor-liquid interfaces", *J. Phys. Chem.*, **100**(31), 13061-13078.
- Osterloh, F.E. (2008), "Inorganic materials as catalysts for photochemical splitting of water", *Chem. Mater.*, **20**(1), 35-54.
- Scofield, J.H. (1976), "Hartree-Slater subshell photoionization cross-sections at 1254 and 1487 eV", *J. Electron. Spectrosc. Relat. Phenom.*, **8**(2), 129-137.
- Vulli, M. and Starke, K. (1978), "Experimental determination of the analyzer brightness of a photoelectron spectrometer", *J. Phys. E. Sci. Instr.*, **10**(2), 158, doi:10.1088/0022-3735/10/2/013.

CC